Chemical Physics Letters 736 (2019) 136811

Contents lists available at ScienceDirect

Chemical Physics Letters

journal homepage: www.elsevier.com/locate/cplett

Research paper

Early time dynamics of laser-ablated silicon using ultrafast grazing incidence X-ray scattering

C. Hull[a,b], S. Raj[a,b], R. Lam[a,b], T. Katayama[c,d], T. Pascal[e], W.S. Drisdell[b,f], R. Saykally[a,b,*], C.P. Schwartz[g,*]

[a] Department of Chemistry, University of California, Berkeley, CA 94720, USA
[b] Chemical Sciences Division, Lawrence Berkeley National Laboratory, Berkeley, CA 94720, USA
[c] Japan Synchrotron Radiation Research Institute (JASRI), 1-1-1 Kouto, Sayo-cho, Sayo-gun, Hyogo 679-5198, Japan
[d] RIKEN SPring-8 Center, 1-1-1 Kouto, Sayo-cho, Sayo-gun, Hyogo 679-5148, Japan
[e] ATLAS Materials Physics Laboratory, Department of NanoEngineering and Chemical Engineering, University of California San Diego, La Jolla, CA 92023, USA
[f] Joint Center for Artificial Photosynthesis, Lawrence Berkeley National Laboratory, Berkeley, CA 94720, USA
[g] Material Sciences Division, Lawrence Berkeley National Laboratory, Berkeley, CA 94720, USA

HIGHLIGHTS

- Grazing incidence geometry yields scattering from only the laser excited regions of the substrate.
- Fragmentation in the ablation plume is seen to occur on a timescale of 20 ps after laser ablation.
- Small angle scattering can be used as a tool to characterize the evolution of nanostructures in the ablation plume.

ABSTRACT

Controlling the morphology of laser-derived nanomaterials is dependent on developing a better understanding of the particle nucleation dynamics in the ablation plume. Here, we utilize the femtosecond-length pulses from an x-ray free electron laser to perform time-resolved grazing incidence x-ray scattering measurements on a laser-produced silicon plasma plume. At 20 ps we observe a dramatic increase in the scattering amplitude at small scattering vectors, which we attribute to incipient formation of liquid silicon droplets. These results demonstrate the utility of XFELs as a tool for characterizing the formation dynamics of nanomaterials in laser-produced plasma plumes on ultrafast timescales.

1. Introduction

The behavior of solids following ultrafast laser irradiation has garnered considerable attention, driven by the growing interest in using ultrafast lasers as tools for synthesis and manipulation of electronic materials. Materials of both scientific and economic interest can be synthesized via laser irradiation, including nanoparticles [1–3], thin films [4], and carbon nanotubes and Fullerenes [5–7]. Laser-based methods are attractive for the production of such materials as they are fast, compatible with a wide variety of different materials, and, unlike other synthesis methods, usually do not require multistep reactions or extensive purification steps [8] to achieve the desired product. A major impediment with pulsed laser synthesis, however, is the difficulty in producing uniform products with selective control over the final morphology, phase and composition. For example, gold nanoparticles synthesized using the "pulsed laser ablation in water" approach display a much higher degree of poly-dispersity than do particles manufactured using more traditional wet chemistry techniques. This makes them undesirable for uses wherein control over the size is critical [9]. To facilitate the use of laser synthesis in the large-scale manufacture of the materials, a more detailed understanding of the entire process of ablation and material condensation is necessary [10]. The ablation process itself is complex, with multiple modes of material removal, including fragmentation, vaporization, explosive boiling, and spallation [10–12]. Both the structure of the plume and its thermodynamic pathways are directly related to the properties of the initial substrate [10,13], the power of the incident laser radiation [14], and the environment in which the synthesis is performed, e.g. vacuum or liquid [7]. The composition of the ablation plume is similarly complex, made up of multiple species, including monomers and ions, small clusters and

* Corresponding authors at: Department of Chemistry, University of California, Berkeley, CA 94720, USA (R. Saykally). The Molecular Foundry, Lawrence Berkeley National Laboratory, Berkeley, CA 94720, USA (C.P. Schwartz).
E-mail addresses: saykally@berkeley.edu (R. Saykally), cpschwartz@lbl.gov (C.P. Schwartz).

https://doi.org/10.1016/j.cplett.2019.136811
Received 5 August 2019; Received in revised form 25 September 2019; Accepted 29 September 2019
Available online 30 September 2019
0009-2614/ © 2019 Elsevier B.V. All rights reserved.

large liquid droplets, all emitted with different time and velocity scales. Understanding the interaction among these different constituents is critical to controlling the final product morphology.

The key to resolving these issues lies in attaining a better understanding of the post-ablation physics via direct experimental characterization. Observation of the earliest steps in plume formation has proven to be a challenge however, as the short length- and time-scales of the process make the experiments difficult [15]. The melted material initially has a thickness only on the order of the optical depth of the material (less than 100 nm), requiring measurement techniques with high surface specificity. Furthermore, the time scale for condensation is also relatively short, ~50 ps in vacuum. Few techniques have the combined spatial and temporal resolution necessary to directly observe the sub-nanosecond dynamics of the melt and resultant ablation plume. Optical techniques have been a popular tool in imaging and spectroscopy of ablation plumes [16–18]. By measuring the emission or absorption spectra of the plume, the components comprising it can be identified. Rough velocity measurements of the plume constituents can also be obtained by imaging only small slices of the plasma at different distances from the substrate as a function of time. Due to the nanosecond measurement timescales and millimeter spatial resolution achieved in such experiments, however, they often provide only limited insight into the actual formation mechanism of the observed particles. Time of flight mass spectrometry has also been utilized to characterize the composition of the plasma plume [19,20] and can provide more detailed measurements of the velocities of the various plume constituents, as well as the cluster sizes in the plasma. This technique is limited by poor time resolution and cannot be used to measure dynamics of cluster formation or growth. In both approaches, the details of nanomaterial nucleation and growth can only be indirectly inferred.

X-ray diffraction is well-suited to carrying out direct characterization of the clusters in the plume and has been used in the past to study nanoparticle formation following laser ablation of gold targets with a nanosecond laser [21]. Based on the small angle scattering pattern observed, the formation of both primary nanoparticles (8–10 nm diameter) and secondary nanoparticles with average diameters of 45 nm were reported. However, the scattering measurements in that experiment were only taken at a time point of ~100 μs after laser irradiation-long after the initial particle formation. Observation of the initial particle formation using modern synchrotron sources would be precluded, as these light sources have pulse durations on the order of tens of picoseconds. Tabletop X-ray sources can achieve the desired femtosecond time resolution but lack the requisite photon flux.

In this study, we sought to observe the earliest dynamics in the femtosecond ablation of silicon by time-resolved grazing incidence X-ray scattering measurements with an X-ray free electron laser. as femtosecond pulses available from the XFEL have the requisite time resolution and intensity to directly observe the earliest stages of the ablation process. We overcome the penetration depth mismatch problem by carrying out the measurement in a total external reflection grazing incidence geometry. In doing so, we limit the penetration depth of the x-ray pulse to the uppermost few nm of the laser irradiated sample, allowing direct observation of only the incipient ablation plume and the formation of particles on a timescale previously unavailable to x-ray scattering.

2. Experimental

Experiments were carried out at the Beamline 3 [22,23] of the SACLA (SPring-8 Angstrom Compact Free Electron LAser) XFEL [24] at the SPring-8 facility. Fig. 1 is a schematic of the experimental design. The 1 mm thick silicon wafers used as samples in the experiment were mounted on a diffractometer stage with XYZ translation capability. X-ray pulses (10 fs, 10 keV) from SACLA impinged on the sample silicon's (1 0 0) face at a 0.1° incident angle, well below the calculated critical angle of 0.17°, ensuring total external reflection of the x-ray beam. For

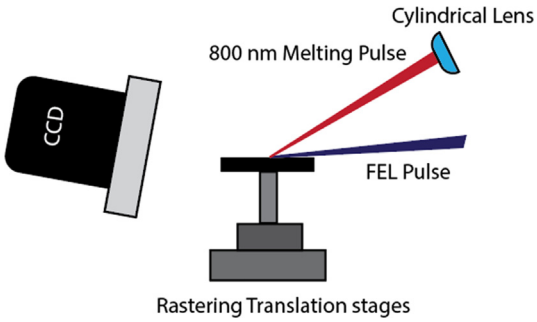

Fig. 1. Experimental design for grazing incidence scattering experiments. The sample is mounted on a diffractometer and aligned at grazing incidence relative to the X-ray pulse. The FEL pulse, focused by Kirkpatrick-Baez mirrors, is spatially overlapped with an 800 nm optical pulse, focused with a cylindrical lens. The sample was rastered perpendicular to both the sample surface and travel direction of the laser propagation. Use of the grazing incidence geometry limits the penetration of the x-ray beams to only the uppermost few nanometers of the sample; as the penetration depth for the optical pulse I on the order of 100 nm, this ensures only the optically-pumped portion of the sample is probed.

the 10 keV x-ray used in the experiment, we estimate the penetration depth to be 4–6 nm into the sample [25]. The diameter of the incident x ray beam was 2 μm, which spread to a final on-sample footprint of ~1 mm length. The shallow angle of incidence also introduced ~1 ps of temporal smearing.

Ablation of the silicon target was performed using a Ti:Sapphire laser (λ = 800 nm, τ = 40 fs, F = 1.0 J/cm^2). The laser pulses were focused onto the sample at a 70° angle relative to surface normal using a cylindrical lens, resulting in an optical spot size that was 2 mm long by 35 μm wide, sufficiently large to ensure complete spatial overlap with the x-ray pulse. The incident fluence of the optical laser was sufficient to ensure complete melting of the probed region. Between each laser shot, the silicon sample was rastered to ensure that each measurement was conducted on a pristine surface. Optical and XFEL repetition rates were restricted to 1 Hz to ensure sufficient time between shots for sample translation.

X-ray scattering patterns were collected for the unmelted sample and at 10 and 20 ps following excitation by the optical laser. Scattering intensity as a function of scattering angle was measured with a MPCCD (multi-port charge-coupled device) set at a working distance of 155 mm from the sample surface [26]. The CCD was subsequently scanned to obtain a q range of 0.25 to 2.4 Å^{-1}. Unmelted patterns were also taken at beamlines 2–1 and 10–2 of the Stanford Synchrotron Radiation Lightsource (SSRL) for comparison but exhibited no noticeable features over the angle range studied here.

3. Results/discussion

Fig. 2 shows the difference in scattering patterns between the pumped and unpumped silicon target at times of 10 and 20 ps following the arrival of the optical laser pulse. For the first 10 ps following laser irradiation, the scattering is largely unchanged, remaining nearly identical to that of the pristine silicon sample. At 20 ps after the optical pulse, a dramatic shift in the scattering pattern is observed. The scattering intensity at low values increases by over an order of magnitude. Scattering intensity in this region is associated with the development of inhomogeneity on the nanoscale, usually associated with nanoparticles and structures. The large increase in scattering intensity at t = 20 ps is thus assigned to nanoscale sized objects that form in the ablation plume. Due to experimental limitations, we did not collect data at q values low enough for accurate modeling, which precludes a complete analysis and characterization of the scattering objects. Nevertheless, the magnitude of the intensity increase is compelling, and we can infer some interesting details as to the carrier of the observed scattering

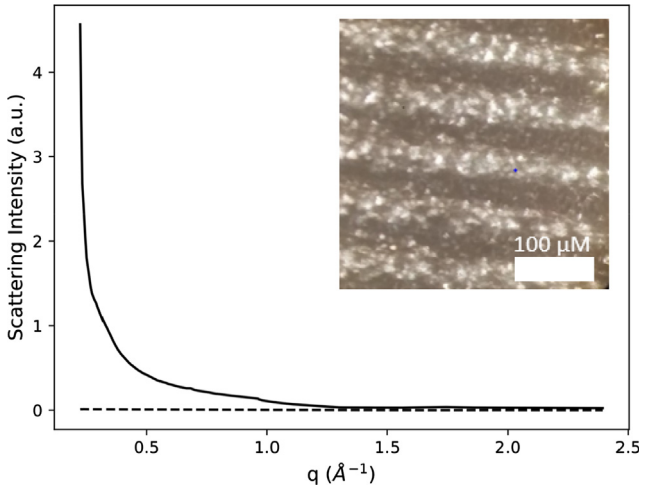

Fig. 2. Main - X-ray scattering intensity measured from q = 0 0.25 to q = 2.4 Å^{-1} at times of 10 ps (dashed) and 20 ps (solid) after irradiation with a fs laser. The scattering pattern for the pristine silicon has been background-subtracted to highlight the impact of the ablation. While the scattering signal at 10 ps is quite similar to that of the unpumped sample, after 20 ps a large increase in scattering intensity is observed, attributed to the formation of liquid silicon droplets in the ablation plume. Inset: Optical microscopy images of the silicon after laser ablation. The bright stripes are the ablation craters left over from interaction with the optical laser. As can be seen in the image, the spots are well-separated, ensuring that a fresh silicon surface was irradiated with every laser shot.

signal.

Based on similarities to other studies [27,28], we assign the scattering intensity increase seen at 20 ps to the formation of large liquid silicon droplets in the ablation plume as it expands. The inset of Fig. 2 shows optical microscope images of the sample surface after interaction with the optical laser. As can be seen from the presence of ablation craters on the surface at 1.0 J/cm^2 fluence, we are clearly in the ablation regime for silicon. It has been observed that after laser irradiation of sufficient intensity, silicon transitions to a liquid metallic state, as evidenced by the increase in the sample's optical reflectivity for laser fluences above ~0.14 J/cm^2, [29]. Initially in a high temperature and pressure state, the plasma expands and cools, eventually crossing the spinoidal line in the phase diagram, which results in fragmentation via the homogenous nucleation of gaseous bubbles throughout the liquid [11,30,31]. This process, known as *phase explosion*, is well-known to be important in the ablation of semiconductors after femtosecond irradiation, and has been observed in both experiments and theoretical investigations of the ablation process [4,32]. The 20 ps timescale observed in this experiment for the appearance of ablation-derived droplets agrees well with previous experimental observations of silicon ablation, wherein it was also observed that reflectivity loss due to the ablation occurred between 10 and 50 ps for the silicon (1 1 1) surface [33]. Additionally, simulations of femtosecond laser ablation of solids show that when the ablating laser fluence is significantly above the ablation threshold, the onset of fragmentation due to void coalescence occurs on a similar tens of ps timescale [11]. Thus, it is quite probable that we sampled the very earliest steps in the liquid ablation process, with the observed droplets being related to the subsequently formed nanoparticles. As semiconductor ablation plumes are known to maintain optically smooth interfaces throughout the ablation process, it is possible to maintain the grazing incidence condition throughout the entirety of the material ablation [30,34]. As such, the experiment is only sensitive to a narrow slice at the outermost surface of the ablation plume. In future experiments, this fact may assist modelling of the thermodynamic conditions of the plume and relating them to the evolution of nanoparticles in the plume, as evidenced by the x-ray scattering. While the two time points collected in this experiment are insufficient for a thorough analysis of the plume dynamics, the experimental techniques developed here establish the viability of exploiting XFEL-based grazing incidence small angle x-ray scattering experiment as a tool for studying ablation dynamics. The use of a grazing incidence geometry results in a probe that is highly selective to the plume itself, thus mitigating interference from the sample bulk. As small angle scattering is a sensitive tool for studying both nanoparticle size and morphology, it is well-suited to studying the formation dynamics of nanostructures in the plume on the ultrafast timescales enabled via use of an XFEL. Additionally, by tuning parameters such as laser fluence, gas pressure around the sample, and the nature of the substrate, a more complete understanding of how these important variables affect shape and properties of the resulting nanomaterials can be achieved.

4. Conclusions

We have employed grazing incidence hard x-ray scattering using an ultrafast free electron laser source to study the earliest time points in the laser ablation of a silicon target. The dramatic rise in scattering intensity observed at low q in the experiment is attributed to the formation of nanoscale droplets of liquid silicon, derived from phase explosion in the laser-prepared liquid. Grazing incidence x-ray scattering shows considerable promise as a tool for studying the ablation dynamics of laser irradiated substrates and the formation of nanoparticles. The technique can be easily extended to other materials, conditions, and time delays. This is significant, as very few experiments have been able to directly measure the properties of the ablation plume on ultrafast timescales. In future work, we hope to study the scattering over broader angle and time ranges, effecting the direct study of both the growth and structural composition of the nanomaterials in the ablation plumes. As the current experiment used only a melting fluence of 1 J/cm^2, future experiments must also explore the melting fluence dependence of the ablation plume dynamics. This will facilitate a deeper understanding of the factors controlling the properties and morphology of nanomaterials produced by laser ablation, and will provide a valuable complement to the femtosecond second harmonic generation [35] and two-photon absorption [36] experiments that we recently demonstrated with free electron laser sources in the soft X-ray region.

Declaration of Competing Interest

The authors declare that they have no known competing financial interests or personal relationships that could have appeared to influence the work reported in this paper.

Acknowledgements

This work is supported by the U. S. Army Research Laboratory and the U. S. Army Research Office under grant number W911NF-13-1-0483 and No. W911NF-17-1-0163. The XFEL experiments were performed at BL3 of SACLA with the approval of the Japan Synchrotron Radiation Research Institute (JASRI) (Proposal No. 2017B8072). S. L. R. received a National Science Foundation Graduate Research Fellowship under Grant No. DGE 1106400. Any opinions, findings, and conclusions or recommendations expressed in this material are those of the author(s) and do not necessarily reflect the views of the National Science Foundation. RKL and RJS were supported by the Office of Science, Office of Basic Energy Sciences, Division of Chemical Sciences, Geosciences, and Biosciences of the U.S. Department of Energy at the Lawrence Berkeley National Laboratory under Contract No. DE-AC02-05CH11231 (LBNL). T.A.P was supported by the molecular foundry. W. S. D. was supported by the Joint Center for Artificial Photosynthesis, a Department of Energy Energy Innovation Hub supported through the Office of Science of the U.S. Department of Energy under Award No.

DE-SC0004993. Use of the Stanford Synchrotron Radiation Lightsource, SLAC National Accelerator Laboratory, is supported by the U.S. Department of Energy, Office of Science, Office of Basic Energy Sciences under Contract No. DE-AC02-76SF00515. Finally, we warmly thank Heather Whitley and Rebecca Lindsey for helpful discussions.

References

[1] F. Mafuné, J.-Y. Kohno, Y. Takeda, T. Kondow, Formation of stable platinum nanoparticles by laser ablation in water, J. Phys. Chem. B 107 (2003) 4218.
[2] M. Kim, S. Osone, T. Kim, H. Higashi, T. Seto, Synthesis of nanoparticles by laser ablation: a review, KONA Powder Part. J. 34 (2016) 80.
[3] A.V. Kabashin, M. Meunier, Synthesis of colloidal nanoparticles during femtosecond laser ablation of gold in water, J. Appl. Phys. 94 (2003) 7941.
[4] M.N.R. Ashfold, F. Claeyssens, G.M. Fuge, S.J. Henley, Pulsed laser ablation and deposition of thin films, Chem. Soc. Rev. 33 (2004) 23.
[5] L. Basso, et al., An all-optical single-step process for production of nanometric-sized fluorescent diamonds, Nanoscale 10 (2018) 5738.
[6] A. Hu, M. Rybachuk, Q.B. Lu, W.W. Duley, Direct synthesis of sp -bonded carbon chains on graphite surface by femtosecond laser irradiation, Appl. Phys. Lett. 91 (2007) 1.
[7] Koji Sugioka, A.P. Michel Meunier, Laser Precis. Microfabri. (2010).
[8] N.G. Semaltianos, Nanoparticles by laser ablation, Crit. Rev. Solid State Mater. Sci. 35 (2010) 105.
[9] S. Besner, A.V. Kabashin, F.M. Winnik, M. Meunier, Ultrafast laser based & green synthesis of non-toxic nanoparticles in aqueous solutions, Appl. Phys. A 93 (2008).
[10] V. Amendola, M. Meneghetti, What controls the composition and the structure of nanomaterials generated by laser ablation in liquid solution? Phys. Chem. Chem. Phys. 15 (2013) 3027.
[11] D. Perez, L.J. Lewis, Ablation of solids under femtosecond laser pulses, Phys. Rev. Lett. 89 (2002) 255504.
[12] A. Cavalleri, K. Sokolowski-Tinten, J. Bialkowski, M. Schreiner, D. Von Der Linde, Femtosecond melting and ablation of semiconductors studied with time of flight mass spectroscopy, J. Appl. Phys. 85 (1999) 3301.
[13] S.L. Johnson, et al., Bonding in liquid carbon studied by time-resolved X-ray absorption spectroscopy, Phys. Rev. Lett. 94 (2005) 57407.
[14] E.G. Gamaly, A.V. Rode, B. Luther-Davies, V.T. Tikhonchuk, Ablation of solids by femtosecond lasers: ablation mechanism and ablation thresholds for metals and dielectrics, Phys. Plasmas 9 (2002) 949.
[15] T.E. Glover, Hydrodynamics of particle formation following femtosecond laser ablation, J. Opt. Soc. Am. B-Opt. Phys. 20 (2003) 125.
[16] S. Noël, J. Hermann, T. Itina, Investigation of nanoparticle generation during femtosecond laser ablation of metals, Appl. Surf. Sci. 253 (2007) 6310.
[17] O. Albert, S. Roger, Y. Glinec, J.C. Loulergue, J. Etchepare, C. Boulmer-Leborgne, J. Perrière, E. Millon, Time-resolved spectroscopy measurements of a titanium plasma induced by nanosecond and femtosecond lasers, Appl. Phys. A 76 (2003) 319.
[18] S. Amoruso, G. Ausanio, M. Vitiello, X. Wang, Infrared femtosecond laser ablation of graphite in high vacuum probed by optical emission spectroscopy, Appl. Phys. A 81 (2005) 981.
[19] H. Varel, M. Wähmer, A. Rosenfeld, D. Ashkenasi, E.E.B. Campbell, Femtosecond laser ablation of sapphire: time-of-flight analysis of ablation plume, Appl. Surf. Sci. 127 (1998) 128.
[20] A.V. Bulgakov, I. Ozerov, W. Marine, Cluster emission under femtosecond laser ablation of silicon, Thin Solid Films 453 (2004) 557.
[21] S. Ibrahimkutty, P. Wagener, A. Menzel, A. Plech, S. Barcikowski, Nanoparticle formation in a cavitation bubble after pulsed laser ablation in liquid studied with high time resolution small angle x-ray scattering, Appl. Phys. Lett 101 (2012) 103104.
[22] K. Tono, et al., Beamline, experimental stations and photon beam diagnostics for the hard x-ray free electron laser of SACLA, New J. Phys. 15 (2013) 83035.
[23] S. Owada, T. Togashi, M. Yabashi, X-ray optics for advanced ultrafast pump – probe X-ray experiments at SACLA Tetsuo Katayama, Takashi Hirano, Yuki Morioka, Yasuhisa Sano, Taito, J. Synchr. Rad. 26 (2019) 333.
[24] T. Ishikawa, et al., A compact X-ray free-electron laser emitting in the sub-ångström region, Nat. Photon. 6 (2012) 540.
[25] B.L. Henke, E.M. Gullikson, J.C. Davis, X-ray interactions: photoabsorption, scattering, transmission, and reflection at E = 50–30,000 eV, Z = 1–92, At. Data Nucl. Data Tables 54 (1993) 181.
[26] T. Kameshima, et al., Development of an X-ray pixel detector with multi-port charge-coupled device for X-ray free-electron laser experiments, Rev. Sci. Instrum. 85 (2014) 33110.
[27] M. Bagge-Hansen, et al., All-angle x-ray scattering during detonation of the high explosive hexanitrostilbene, J. Appl. Phys 117 (2015) 245902.
[28] T.M. Willey, et al., Measurement of carbon condensates using small-angle x-ray scattering during detonation of high explosives, AIP Conf. Proc. 1793 (2015) 30012.
[29] K. Sokolowski-Tinten, D. von der Linde, Generation of dense electron-hole plasmas in silicon, Phys. Rev. B 61 (2000) 2643.
[30] K. Sokolowski-Tinten, et al., Transient states of matter during short pulse laser ablation, Phys. Rev. Lett. 81 (1998) 224.
[31] A. Cavalleri, K. Sokolowski-Tinten, J. Bialkowski, M. Schreiner, D. von der Linde, Femtosecond melting and ablation of semiconductors studied with time of flight mass spectroscopy, J. Appl. Phys. 85 (1999) 3301.
[32] J.H. Yoo, O.V. Borisov, X. Mao, R.E. Russo, Existence of phase explosion during laser ablation and its effects on inductively coupled plasma-mass spectroscopy, Anal. Chem. 2288 (2001).
[33] K. Sokolowski-tinten, et al., Dynamics of femtosecond-laser- induced ablation from solid surfaces, SPIE 3343 (2019) 46.
[34] D. von der Linde, K. Sokolowski-Tinten, J. Bialkowski, Laser–solid interaction in the femtosecond time regime, Appl. Surf. Sci. 109 (1997) 1.
[35] R.K. Lam, et al., Soft X-ray second harmonic generation as an interfacial probe elettra-sincrotrone trieste, Phys. Rev. Lett. 120 (2018) 23901.
[36] R.K. Lam, et al., Two-photon absorption of soft X-ray free electron laser radiation by graphite near the carbon K-absorption edge, Chem. Phys. Lett. 703 (2018) 112.